Total energies in Se. III. Defects in the glass

David Vanderbilt
Department of Physics, University of California at Berkeley, Berkeley, California 94720

J. D. Joannopoulos
Department of Physics, Massachusetts Institute of Technology, Cambridge, Massachusetts 02139

(Received 7 September 1982)

The effective Hubbard U for the bonding coordination defect in glassy Se is investigated. This is accomplished by applying local-density total-energy calculations directly to charged defects in a superlattice configuration. The existence of a large negative contribution to U, arising from interconversion between dangling-bond and threefold-coordinated structures, is confirmed. However, a still larger Coulomb repulsion gives rise to an overall *positive* U.

I. INTRODUCTION

Glassy Se, together with a variety of compound glasses, comprise a class of materials known as the chalcogenide glasses. These materials have a number of interesting experimental properties in common,[1–6] including similar features in the luminescence, photoinduced electron spin resonance (ESR), and photoinduced ir absorption.[5,6] Most curious, however, is the fact that experiments appear to imply a large density of states ($\sim 10^{17}$ cm^{-3} eV^{-1}) pinning the Fermi level near midgap,[1–3] while the number of free spins is much smaller ($\lesssim 10^{15}$ cm^{-3}).[1–5]

Several years ago, Anderson[7] made a novel proposal to explain the quenching of the spins in these materials. He suggested that a strong electron-phonon coupling could give rise to a negative effective Hubbard correlation energy ("negative U") which would tend to pair free spins in the material. Mott, Davis, and Street[8] and Kastner, Adler, and Fritzsche[9] then incorporated Anderson's idea into a defect model, in which intrinsic bonding defects are responsible for the negative U. Other authors have proposed competing models based upon a broad distribution of bond strengths[10,11] or upon polarons[12] to explain the experiments.

The defect model is illustrated schematically for Se in Fig. 1. The bulk structure, Fig. 1(a), was assumed to be a continuous random network, composed of long chains and perhaps some rings. When a chain is broken, a dangling bond results; simple counting arguments imply that the resulting one-fold-coordinated defect will be negatively charged when the valencelike states are all filled. We use the notation D^- to indicate the *charge* state, and the notation C_1^- to denote the relaxed *structure* for that charge state (the subscript indicates the coordination number). The C_1^- defect is shown in Fig. 1(b). If two electrons are successively removed from D^- to create D^0 and D^+, Figs. 1(c) and 1(d), structural relaxation was expected to take place. In particular, the D^+ was expected to form a cross-linked structure C_3^+ (Ref. 9). This structural relaxation was thought to be responsible for a negative U_{eff}. Previous work has indicated that the D^0 remains singly coordinated, i.e., C_1^0 (Ref. 13), and that both one-fold- and three-fold-coordinated defects give rise to deep-gap states.[14]

Unfortunately, compelling theoretical arguments for the existence of the negative U for the defects in the defect model were absent; simple models[9] could not predict the sign of U for defects in a chalcogenide material. The lack of long-range order and symmetry, the necessity of fully relaxing the defect structures, and the difficulty of dealing with charged defects all presented serious obstacles to the

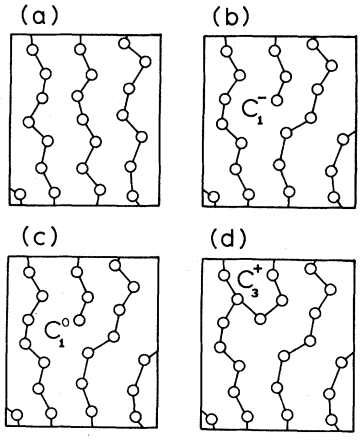

FIG. 1. Schematic illustration of defect model for g-Se. (a) Bulk glass. (b) Negatively charged coordination defect. (c) Neutral coordination defect (here shown singly coordinated). (d) Positively charged coordination defect.

formulation of a realistic theory.

Here, we show that the key to overcoming these obstacles is the development of tractable but realistic *ab initio* total-energy calculations for semiconductors. Firstly, the effective U may easily be written in terms of total energies. Let C_3^+, C_1^0, and C_1^- represent the relaxed defect with charges $+1$, 0, and -1, respectively. Then the energy level for adding the first electron to the defect state is defined as

$$\epsilon_1 = E_{\rm tot}(C_1^0) - E_{\rm tot}(C_3^+) , \tag{1a}$$

while that for adding the second is

$$\epsilon_2 = E_{\rm tot}(C_1^-) - E_{\rm tot}(C_1^0) . \tag{1b}$$

The effective U is just $\epsilon_2 - \epsilon_1$, or

$$U_{\rm eff} = E_{\rm tot}(C_1^-) + E_{\rm tot}(C_3^+) - 2E_{\rm tot}(C_1^0) . \tag{2}$$

Secondly, the total-energy formalism allows one to find the fully relaxed defect structure for each charge state by minimizing the total energy with respect to structural degrees of freedom.

This paper is the third in a series. The first[15(a)] (hereafter referred to as paper I) demonstrated that accurate structural information on trigonal Se may be obtained from total-energy calculations using local-density theory and first-principles pseudopotentials. The second[15(b)] (paper II) extended the method to supercell structures containing a vacancy, thereby showing that systems of low symmetry can be treated as well. In particular, the use of a dielectric matrix approach to obtain fast electronic self-consistency, and the use of Hellman-Feynman forces to obtain fast convergence upon the structural minimum, were shown to be crucial for these supercell calculations.

In this paper, the same techniques are applied to estimate the effective Hubbard U of the defect model for the case of pure glassy Se. Superlattice structures, similar to those of paper II, are again used. The major extension of this work is to overcome several difficulties associated with *charged* defects, and to eliminate interdefect interactions within the superlattice structure. Having done so, we are able to obtain the equilibrium structural configuration for each of the three charge states D^+, D^0, and D^-, and a value for $U_{\rm eff}$ as given by Eq. (2). We find that $U_{\rm eff}$ is *positive,* despite a large negative contribution coming from structural relaxation.

A discussion of the superlattice structures that were used to model the defects is given in Sec II, along with a discussion of the methods for handling charged defects and for eliminating interdefect interactions. Section III contains the results for the structure and electronic states of the D^+, D^0, and D^-, and for $U_{\rm eff}$. In Sec. IV, the implications of the present results are considered in the context of the experimental work on chalcogenide glasses. Section V contains a summary and conclusions.

II. THE METHOD

In order to model the defects of Fig. 1, we have constructed superlattice structures containing the defects of interest. Purely topological considerations imply that any supercell must contain two (or more precisely, an even number of) coordination defects of the sort shown in Figs. 1(b)–1(d). Moreover, the supercell must contain a net charge of zero, lest long-range Coulomb interactions give rise to divergences in the potential. Therefore, the natural approach is to consider a supercell which may contain either two C_1^0 defects, or one C_3^+ and one C_1^-. From Eq. (2), we then have

$$U_{\rm eff} = E_{\rm tot}(C_3^+ C_1^-) - E_{\rm tot}(2C_1^0) , \tag{3}$$

where $(2C_1^0)$ is the supercell containing a pair of neutral defects, and $(C_3^+ C_1^-)$ is the same cell with the atoms displaced to form a pair of oppositely charged defects.

Figure 2 shows two superlattice structures which we have used to model the defects. The superlattice of Fig. 2(a) (hereafter referred to as geometry I) is identical with that used to study vacancies in paper II; it contains eight atoms per cell. The superlattice

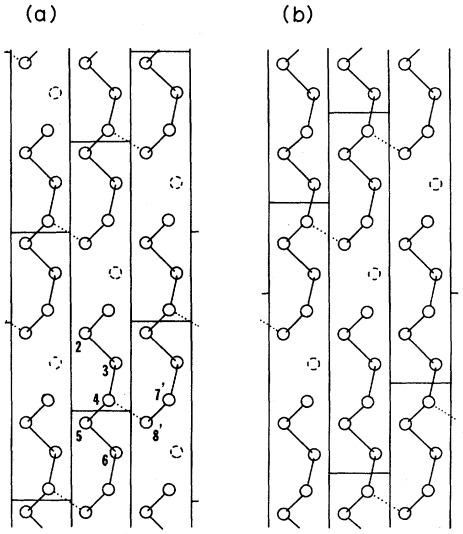

FIG. 2. Superlattice structures used to model defects, made by starting with trigonal crystal structure and removing certain atoms (dashed circles) to create defects. (a) Geometry I. (b) Geometry II. (Dotted lines are extraordinary bonds which form when modeling threefold structures. Certain atoms are labeled with numbers to facilitate discussion in Sec. III.)

of Fig. 2(b) (hereafter geometry II) differs in that it contains 11 atoms per cell. Moreover, the staggering of the chains with respect to neighboring layers (out of the plane of Fig. 2) differs between geometries I and II. The latter was chosen as an alternate geometry because it minimizes the importance of interdefect Coulomb interactions, to be discussed below. The lattice vectors of geometry I are

$$\vec{a}_{\rm I}=\left[-\frac{1}{2},-\frac{a\sqrt{3}}{2},-c\right],$$
$$\vec{b}_{\rm I}=\left[-\frac{a}{2},\frac{a\sqrt{3}}{2},-c\right], \tag{4a}$$
$$\vec{c}_{\rm I}=(a,0-c)\ .$$

in the notation of paper II, while those of geometry II are

$$\vec{a}_{\rm II}=(a,0,0)\ ,$$
$$\vec{b}_{\rm II}=\left[-\frac{a}{2},\frac{a\sqrt{3}}{2},-c\right], \tag{4b}$$
$$\vec{c}_{\rm II}=(0,a\sqrt{3},2c)\ .$$

Either geometry I or II alone could be used to study the interconversion between $(2C_1^0)$ and $(C_3^+C_1^-)$, by breaking or forming the extraordinary bond indicated as a dotted line in Fig. 2. We have carried out calculations on *both* of the supercell geometries in order to ensure that the details of the geometry, in particular the interchain coupling configuration, do not crucially affect the results.

The scheme of the present calculations is very similar to that used in paper II. For each of the two supercell geometries I and II, and for each of the two charge states D^0D^0 and D^+D^-, the total energy and Hellman-Feynman forces are calculated. The Born—von Kármán force constant model discussed in paper II is then used to predict atom displacements which relieve the forces. The process is iterated until the structure is fully relaxed. This determines the relaxed geometries C_3^+, C_1^0, and C_1^-. Finally, $U_{\rm eff}$ is given from Eq. (3).

Several new problems arise, however, in the present instance. Most importantly, the energies which appear in Eq. (2) are the energies of isolated defects. That is, $E_{\rm tot}(C_1^-)$ is properly the energy of a C_1^- defect embedded in an infinite continuous random network. The energies which appear in Eq. (3), on the other hand, are those of defects in a superlattice structure containing a large density of other defects. Thus any interactions between defects in the superlattice structure will give rise to spurious contributions to the total energy, which should be eliminated in order to estimate the true $U_{\rm eff}$. There are three important interdefect interactions which must be eliminated: These are (1) the hopping matrix elements which give rise to hybridization among the defect states on neighboring defects; (2) the Coulomb interactions between the charge clouds of different charged defects; (3) the effects of spin polarization which must be introduced to model isolated D^0 defects.

An additional problem which arises in this work is that the traditional local-density calculations do not allow charge transfer (e.g., from D^+ to D^-) to be treated as an *input* to the calculation. Rather, the structural configuration determines the electronic ground state and in turn the charge configuration. In our case, we would like to minimize the total energy with the charge configuration *constrained,* to D^0D^0 (or to D^+D^-) in order to find the relaxed geometry for the D^0 (or D^+ and D^-) defect.

This latter problem and the elimination of the interdefect interactions arising from hopping matrix elements between defect states, are solved simultaneously by employing a density-matrix approach to the occupations of the electronic states. This method has been described and justified in detail elsewhere,[16] but a brief summary is given here.

Each of the two defects in the unit cell has a midgap defect state; label these ψ_1 and ψ_2. At each iteration of the self-consistent process, and at each $\vec{k}$ point, the two eigenstates ψ_b and ψ_a corresponding to the "bonding" and "antibonding" combinations of ψ_1 and ψ_2 are identified. In a traditional ground-state energy calculation, ψ_b would be occupied with two electrons, whereas ψ_a would be empty. However, the eigenvalue ϵ_b lies below both ϵ_1 and ϵ_2, lowering the band-structure energy (and the total energy) compared to the case of distant defects which we want to model. Moreoever, we would like to constrain the number of electrons in ψ_1 (or ψ_2) to be 0, 1, or 2, depending on the charge configuration under study.

This is accomplished as follows. First, the states corresponding to ψ_1 and ψ_2 are constructed out of ψ_b and ψ_a by requiring that ψ_1 (ψ_2) be the ψ which maximizes (minimizes) the expectation value

$$\frac{\langle\psi|P_{\Omega_1}-P_{\Omega_2}|\psi\rangle}{\langle\psi|\psi\rangle}\ , \tag{5}$$

where the projection operator P_Ω is defined as

$$P_\Omega=\int_\Omega d^3r\ |r\rangle\langle r| \tag{6}$$

and Ω_1 (Ω_2) is a spherical volume centered on defect site 1 (2). Equation (5) corresponds to a 2×2 eigenvector problem whose solution defines a unitary transformation which connects the *local* basis L (ψ_1 and ψ_2) with the Hamiltonian *eigenstate* basis H (ψ_b

and ψ_a). Second, the electronic occupations are specified by a 2×2 density matrix which is *diagonal* in the *local* representation:

$$\underline{n}^L=\begin{bmatrix} n_1 & 0 \\ 0 & n_2 \end{bmatrix}, \tag{7}$$

where n_1 and n_2 are the desired occupations of ψ_1 and ψ_2. The unitary transformation found above is then used to transform this to the eigenstate representation

$$\underline{n}^H=\begin{bmatrix} n_{bb} & n_{ab} \\ n_{ba} & n_{aa} \end{bmatrix}. \tag{8}$$

The off-diagonal occupation number $n_{ba}=n_{ab}^*$ provides the extra degree of freedom needed to constrain the charge and to obtain the correct total energy in lowest order. Third, the density matrix is implemented by defining the charge density to be

$$\rho(r)=\sum_{ij} n_{ij}\psi_i^*(r)\psi_j(r)\ . \tag{9}$$

The total energy is then the usual local functional of the charge density; it can be rewritten

$$E_{\rm tot}=\sum_i n_{ii}\epsilon_i+\Delta E_{hxc}[\rho]\ , \tag{10}$$

where the functional ΔE_{hxc} is the usual correction term which compensates for the overcounting of electron-electron correlations.

In practice Eqs. (9) and (10) are evaluated in the Hamiltonian eigenstate representation, using (8), but by invariance under basis transformation the result is identical if evaluated in the local representation using (7). The latter makes it transparent that the present approach automatically solves both problems mentioned at the outset: It allows the charge configuration to be treated as an input, and it eliminates the artificial bonding energy which would result if ϵ_b, rather than ϵ_1 and ϵ_2, were occupied.

This density-matrix approach is implemented at a very basic level of the calculation; all quantities, most particularly the Hellman-Feynman forces, are calculated for a given density matrix (i.e., for a given charge configuration). This means that the forces are *different* for D^+D^- vs D^0D^0 even if the structural configuration is held fixed. Thus the forces will guide the structure to a *different* structural equilibrium for the two cases, as desired.

We turn now to the question of eliminating the Coulomb interactions between the charge clouds of charged effects in the superlattice structure. The resulting correction will be referred to as a "Madelung correction," since it is given to lowest order by the Madelung energy of point charges on the lattice of oppositely charged defect sites, embedded in a uniform dielectric. By allowing for the q dependence of the dielectric function $\epsilon(q)$, and by taking into account the extent of the charge clouds, the estimate of the Madelung correction can be improved. The q dependence correction is small, however; by equating $1/r\epsilon(r)$ with the Fourier transform of $1/q^2\epsilon(q)$ for a model dielectric function,[17] it was found that $\epsilon(r)$ approaches to within 95% of $\epsilon(\infty)$ for $r=3.7$ Å. Since the distance between charged defects in the superlattice structures typically exceeds this value, the q-dependence correction was dropped.

The spatial extent of the charge clouds was modeled in terms of Gaussians, rather than point charges. The width σ of the Gaussians $\exp(-|r-R|^2/\sigma^2)$ was adjusted in order to give the best fit to the defect charge densities defined as the difference charge density between the charged D^+D^- and neutral D^0D^0 electronic configuration for a given structural configuration. The width obtained in this way is typically $\sigma\approx2.4$ Å. The Madelung energy is now the electrostatic energy to remove these Gaussian packets to infinity, and may be obtained exactly by combining the appropriate reciprocal space sums and analytic real space integrals. The Madelung energy is typically reduced by about 20% from that of point charges. Any Madelung terms discussed hereafter always include this finite-extent correction.

The Madelung corrections are generally quite sizable, e.g., ~0.8 eV/supercell for $(C_3^+C_1^-)$ in geometry I. Thus any intrinsic errors in the estimates for these terms comprise a major potential source of error in the calculation. For this reason, geometry II was chosen so as to have a smaller Madelung correction, ~0.2 eV/supercell for $(C_3^+C_1^-)$. The difference arises because each negative defect is well screened by surrounding positive defects and vice versa in geometry I, whereas the oppositely charged defects are roughly segregated into layers in geometry II, so that repulsive interactions are more prevalent. Thus any errors arising from the estimate of the Madelung correction will be greatly reduced in geometry II.

The final problem introduced above concerned spin-polarization effects at the neutral defect. The problem does not arise for the charged defects, which have no unpaired spins. By treating the neutral defect in a non-spin-polarized local density formalism, however, we fail to take into account the fact that the unpaired spin on a free D^0 will give rise to an excess of $\rho_\uparrow$ over $\rho_\downarrow$. The resulting spin-polarization (SP) correction is evaluated to first order in perturbation theory by constructing $\rho_\uparrow$ and $\rho_\downarrow$ from the wave functions of the non-spin-polarized calculation, and using the spin-density exchange-correlation functional[18] of Hedin-Lundquist (HL) to

evaluate the difference:

$$\Delta E_{\rm tot}^{\rm SP}=E_{\rm HL}(\rho_\uparrow,\rho_\downarrow)-E_{\rm HL}(\bar{\rho},\bar{\rho})\ , \tag{11}$$

where $\bar{\rho}=(\rho_\uparrow+\rho_\downarrow)/2$. This correction is typically ~ 0.1 eV for a single neutral defect.

In summary, three new corrections are introduced in order to model distant defects using a superlattice configuration. Firstly, the hybridization of the defect states is effectively eliminated, and the charge configuration is chosen, by using a density-matrix formalism which allows off-diagonal occupation numbers. Secondly, for D^+D^- the nonphysical Coulomb (Madelung) interactions between the defects are estimated and subtracted out. Thirdly, the total energy of the neutral D^0D^0 case is adjusted to account for spin-polarization effects.

III. RESULTS

The results for the relaxed structures ($2C_1^0$) and ($C_3^+C_1^-$) are given in Table I. Physical information about the local structure in the vicinity of the three charged defects C_1^-, C_1^0, and C_3^+ is extracted and presented in Table II.

As expected, the negatively charged D^- defect takes on a onefold-coordinated structure (C_1^-). The results for geometries I and II are in close agreement, and indicate that there are only small relaxations away from crystalline bond lengths and angles near the defect site. In particular, the last bond on the chain shortens by $\sim 2\%$, and the last bond angle opens by $\sim 3°$.

The relaxed neutral D^0 defect is found to be structurally almost identical to that of the D^-; it is again a onefold-coordinated structure (C_1^0) with a bond length at the defect site shorter by $\sim 1\%$ than that of C_1^-. Threefold-coordinated structures were also tested, but were found to be higher in energy and to decay directly (i.e., without passing over a barrier) back to C_1^0. However, the energy difference was not large; after approximately two cycles of calculating the forces and adjusting the atom locations, an unstable but roughly relaxed C_3^0 structure was reached with energy only ~ 0.25 eV higher than that of C_1^0. Further cycles drove the structure slowly the rest of the way to C_1^0. These results agree qualitatively with the earlier work of Ref. 13.

In contrast to the extremely small relaxations which take place between D^- and D^0, we confirm that the D^+ defect undergoes a radical reconstruction to form a threefold-coordinated C_3^+ structure. Table II shows that the bond lengths adjoining the threefold-coordinated site are on average 4% longer than the crystalline bond length, and that the bond angles there are typically somewhat smaller. However, the variations from one bond to another, and from geometry I to geometry II, are much greater than for C_1^0 or C_1^-. These differences presumably arise from the need to cross-link the chains and yet retain an efficient packing with respect to neighbor-

TABLE I. Calculated minimum energy superlattice structures for D^0D^0 and D^+D^- charge states. Atom locations τ are in Cartesian coordinates. [Lattice vectors are given in Eq. (4).]

		($2C_1^0$)			($C_3^+C_1^-$)		
Super cell	Atom	τ_x (Å)	τ_y (Å)	τ_z (Å)	τ_x (Å)	τ_y (Å)	τ_z (Å)
I	1	−0.418	−0.830	−1.698	−0.209	−0.795	−1.740
	2	−0.423	0.776	−3.323	−0.328	0.692	−3.494
	3	1.085	0.000	−5.002	1.273	−0.077	−5.081
	4	−0.469	−0.897	−6.649	−0.236	−1.155	−6.875
	5	−0.504	0.832	−8.244	−0.417	0.823	−8.362
	6	1.039	−0.029	−9.866	1.009	−0.007	−10.039
	7	−0.529	−0.764	−11.471	−0.634	−0.751	−11.513
	8	−0.483	0.951	−13.028	−0.667	1.090	−13.011
II	1	−0.493	−0.867	−1.680	0.109	−1.085	−1.836
	2	−0.450	0.809	−3.256	0.050	0.540	−3.503
	3	1.030	−0.004	−4.914	1.547	−0.219	−5.186
	4	−0.449	−0.855	−6.553	0.056	−1.086	−6.823
	5	−0.443	0.856	−8.190	0.077	0.704	−8.423
	6	1.037	0.000	−9.827	1.528	−0.227	−10.082
	7	−0.443	−0.856	−11.464	0.064	−1.269	−11.878
	8	−0.449	0.855	−13.100	0.014	0.659	−13.416
	9	1.030	0.004	−14.739	1.421	−0.257	−15.070
	10	−0.450	−0.809	−16.398	−0.097	−1.081	−16.680
	11	−0.493	0.867	−17.974	−0.519	0.747	−18.128

TABLE II. Calculated minimum energy structures for three charge states of coordination defect in g-Se. Bond lengths refer to bonds adjoining defect site; angles are at neighboring site for C_1 defects, at site itself for C_3. Calculated values for the trigonal crystal (from paper I) are given for comparison.

		Geometry I		Geometry II	
Charge state	Structure	Bond length (Å)	Bond angle (deg)	Bond length (Å)	Bond angle (deg)
D^-	C_1^-	2.30	105.4	2.34	104.4
D^0	C_1^0	2.29	105.5	2.31	105.4
D^+	C_3^+	2.58	97.2	2.52	97.8
		2.48	101.0	2.47	108.7
		2.31	98.3	2.42	97.2
	(Crystal)	(2.37)	(102.6)	(2.37)	(102.6)

ing chains. Since the geometrical relationships between neighboring chains are different for geometries I and II, the variations present in Table II are natural, and presumably reflect the variations to be found in real C_3^+ defects in the glass. Onefold-coordinated structures (C_1^+) were also tested, but were found to be at least 0.5 eV higher in energy and to decay without barrier directly to the C_3^+ structure.

The probability density for the defect states associated with the C_1^-, C_1^0, and C_3^+ defects are shown in Figs. 3–5. The defect state is similar for C_1^- and C_1^0 (Figs. 3 and 4), and for the dangling bonds at the vacancy in paper II. It consists primarily of a π^* combination of nonbonding p orbitals on the last two atoms of the chain, with most of the weight on the final atom, as expected.[14]

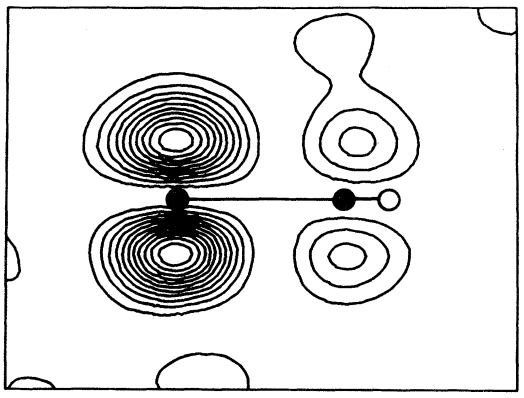

FIG. 3. Probability density for defect state at C_1^-. Plane of plot passes through last two atoms on chain (black circles) and is normal to bond angle with third atom (open circle, out of plane).

The situation is more complicated for the C_3^+. Let $\sigma^*_{4\text{-}3}$ be the σ^*-bond orbital between atoms 4 and 3 of Fig. 2 (see also Table I), and similarly for $\sigma^*_{4\text{-}8'}$, etc. In the simplest picture, we expect the defect state to be a symmetric combination of $\sigma^*_{4\text{-}3}$, $\sigma^*_{4\text{-}5}$, and $\sigma^*_{4\text{-}8'}$. However, the π interactons between, e.g., $\sigma^*_{4\text{-}5}$ and $\sigma^*_{7'\text{-}8'}$ causes a splitting into $\pi(\sigma^*_{4\text{-}5},\sigma^*_{7'\text{-}8'})$ and $\pi^*(\sigma^*_{4\text{-}5},\sigma^*_{7'\text{-}8'})$ states. The lower $\pi(\sigma^*,\sigma^*)$ state is pushed into the gap.[14] For a C_3^+ defect with full threefold symmetry, one therefore expects a defect state corresponding to a symmetric combination of three $\pi(\sigma^*,\sigma^*)$ complexes.

The actual density is shown for the C_3^+ of geometry I in Fig. 5. Only two of the central σ^*-bond orbitals have large amplitude. These are $\sigma^*_{4\text{-}5}$ and $\sigma^*_{4\text{-}8'}$, which have been pushed down by π interactions with $\sigma^*_{7'\text{-}8'}$ and $\sigma^*_{2\text{-}3}$, respectively. $\sigma^*_{4\text{-}3}$ has no available σ^* neighbor with which to form a π complex, and thus does not participate in the defect

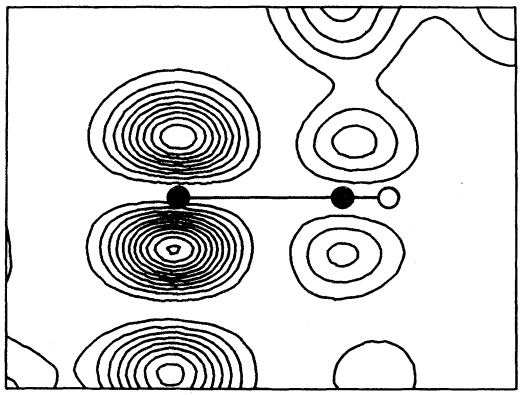

FIG. 4. Probability density for defect state at C_1^0. Geometry is same as that of Fig. 3.

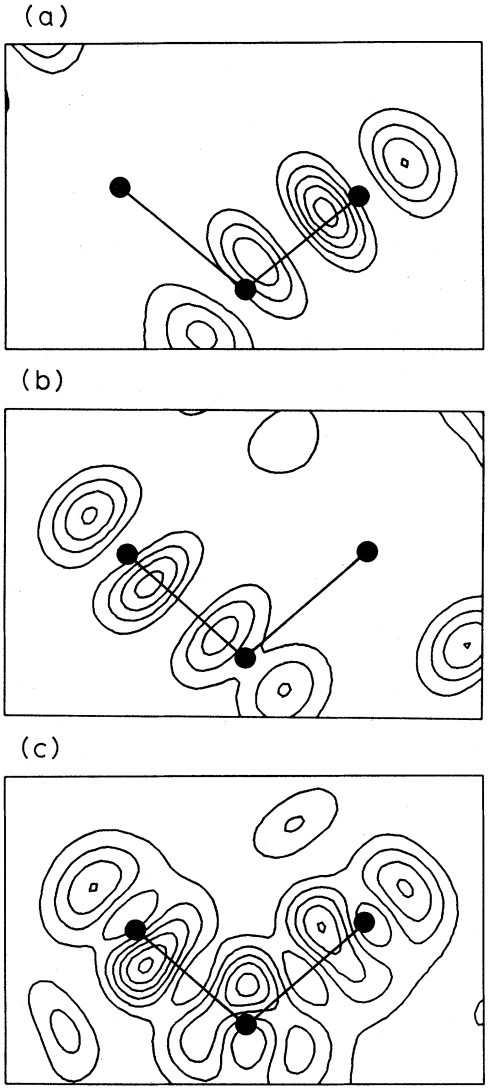

FIG. 5. Probability density for defect state at C_3^+. In each case, plane of plot passes through threefold-coordinated site and two neighbors. (a) Atoms 3-4-8'. (b) Atoms 5-4-3. (c) Atoms 8'-4-5. (Atom labels are from Table I; prime indicates atom from neighboring cell.)

state. These results again emphasize the importance of π interactions in understanding the electronic structure of Se. In any case, the defect state of the C_3^+ is considerably more delocalized than that of the C_1^0 or C_1^-.

We turn now to the results for the total energy, and in particular U_{eff}. The total energy of the relaxed C_1^0 defect is here found to be 0.80 eV measured with respect to the bulk. This can be interpreted as the average energy per defect to create dangling bonds in the glass. The total energies of the C_3^+ and C_1^- are not individually well defined independently of the chemical potential (Fermi level), but the sum of $E_{\text{tot}}(C_3^+)$ and $E_{\text{tot}}(C_1^-)$ can be directly compared with $2E_{\text{tot}}(C_1^0)$ in the manner of Eq. (2), yielding U_{eff}.

The results for U_{eff} are given in Table III. It is found to be $+0.66$ and $+0.35$ eV for supercells I and II, respectively. In order to demonstrate the importance of the various corrections, the total U_{eff} has been broken down into an "uncorrected" U and three corrections ΔU corresponding to the Madelung, density-matrix, and spin-polarization corrections. The uncorrected U is the energy needed to transfer a charge simultaneously in each unit cell of the superlattice structure. This energy still contains the spurious interdefect Coulomb interactions, which are less important for geometry II (see the discussion of the Madelung terms in the preceding section). This is reflected in the values of the Madelung correction in Table III, and explains why the uncorrected U is larger for geometry II than for I. When the Madelung correction is included, a comparison between the U values of geometries I and II becomes physically meaningful; the subtotals are now in closer agreement, ~ 0.8 and 0.6 eV, respectively, with more confidence assigned to the latter value. The density-matrix and spin-polarization corrections are seen to be roughly the same for the two geometries. Even allowing the most unfavorable error estimates, Table III clearly shows a positive overall U in both cases.

While a U of ~ 0.45 eV falls comfortably within both error ranges, it is quite possible that the difference between the U for geometries I and II is real. Some variation in U for defects in the glass should be expected, since the details of the local structural environment will be different for each defect, just as it is different for geometries I and II. If the distribution of U values is very wide, a few may be negative, but the absence of free spins cannot be ex-

TABLE III. Contributions to the effective Hubbard U. Three corrections ΔU correspond to effects of subtracting out interdefect interactions. Error estimates indicate theoretical uncertainty due to sources other than the frozen-core and local-density approximations.

	Geometry I (eV)	Geometry II (eV)
Uncorrected U	0.10±0.12	0.42±0.12
Madelung ΔU	0.71±0.25	0.16±0.04
Density matrix ΔU	−0.34±0.03	−0.39±0.03
Spin-polarized ΔU	0.19±0.02	0.16±0.02
Total corrected U	0.66±0.28	0.35±0.13

plained unless almost all are negative.

To see physically how a positive U comes about, consider the configuration coordinate diagram for a pair of distant defects, shown in Fig. 6. When the charge state is neutral, D^0D^0, the defects relax to the structure $C_1^0C_1^0$. A calculation of the total energy for this same geometry after charge transfer shows that it then costs ~ 1.1 eV to transfer an electron (e.g., optically) from one defect to the other. Most of this energy (~ 0.9 eV) is attributable to the Coulomb repulsion of putting a second electron on the dangling bond of the C_1^-. The system in the D^+D^- charge state then relaxes to the $C_3^+C_1^-$ configuration, lowering its energy by ~ 0.5 eV in the process.

Thus we see that the qualitative features of the defect model are confirmed: The positively charged dangling bond *does* relax to form an extraordinary bond, and this *does* give rise to a negative contribution (~ -0.5 eV) to the effective U. However, the Coulomb interaction gives rise to a larger positive contribution, and to an overall *positive* U_{eff}.

IV. DISCUSSION

In light of these results, how can we understand the experimental puzzle of an apparently well-pinned Fermi level in the absence of free spins in chalcogenides? The key appears to lie in making a careful distinction between g-Se and the other chalcogenides. It is well documented[1–5] that the cold dark density of free spins in annealed samples is $\lesssim 10^{15}$ cm^{-3} for both g-Se and other chalcogenides. On the other hand, space-charge limited current,[19] screening length,[20] and xerographic[21] measurements indicate that Se has an unusually low density of deep midgap states, $\lesssim 2\times 10^{14}$ cm^{-3}, compared to $\sim 10^{17}$ cm^{-3} for the compound chalcogenides.[1–3] Thus for the special case of g-Se, the experiments do not appear to be inconsistent with a positive U.

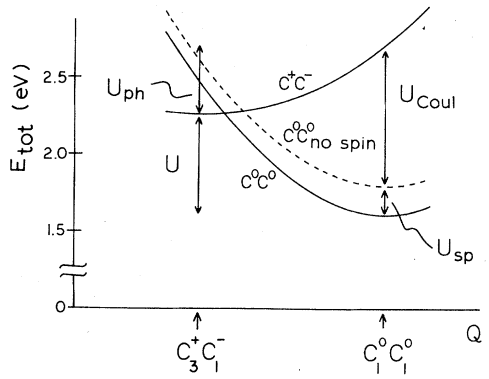

FIG. 6. Configuration coordinate diagram for a distant pair of defects, as derived from geometry I. Solid lines show total energy for neutral and charged cases; dashed line shows neutral case without spin polarization. The total effective U is a sum of positive Coulomb (U_{Coul}) and spin-polarization (U_{sp}) contributons and a negative phonon (U_{ph}) or structural relaxation contribution.

The idea that Se may be peculiar among the chalcogenides in having a positive U is compatible with two interesting differences between Se and the compound chalcogenide glasses. First, g-Se has a relatively low-static dielectric constant of $\epsilon = 6.6$ (Ref. 22) compared, e.g., with 12–20 for the series $As_2Se_xTe_{3-x}$.[23] Second, the defect wave function for C_1 in g-Se is much more localized than, e.g., in g-As_2Se_3.[24] Since the positive Coulomb contribution U_{Coul} to U_{eff} scales as $U_{\text{Coul}} \propto \epsilon^{-1}L^{-1}$, where L is the extent of the defect state, U_{eff} is in fact expected to be more positive in Se than in other chalcogenides. Thus a positive overall U would seem to be quite reasonable for g-Se. Moreover, our results by no means rule out the existence of a negative U in the compound chalcogenide glasses.

While we have calculated U_{eff}, which represents the *difference* between the energy levels ϵ_1 and ϵ_2 of Eq. (1), we have not determined the absolute energy location of the states in the gap. This is because the individual total energies of C_1^- and C_3^+ cannot be sorted out in the calculation of the total energy of the supercell containing both. In principle they might be estimated by a transition-state approach, but this is problematic because the valence- and conduction-band edges are not precisely identifiable in the superlattice calculations, and because the choice of *ab initio* pseudopotentials and other features of the method are optimized to give good total energies rather than good optical excitation energies (e.g., a good gap). Therefore, it is difficult to make direct contact with optical experiments.

Nevertheless, we have sketched in Fig. 7 a possible scenario for the locations of the states in the gap. The *structures* C_1^-, C_1^0, and C_3^+ are defiend to be the relaxed structures for the charge states -1, 0, and $+1$, respectively. Three energy levels are shown for each structure. $\epsilon_{+/0}$ and $\epsilon_{0/-}$ are the *optical* excitation energies to add the first and second electrons to the defect, respectively, holding the structure fixed. These could be approximated by transition-state calculations for the $+\frac{1}{2}$ and $-\frac{1}{2}$ charge states respectively. The local-density one-electron eigenvalue ϵ_0 of the neutral charge state, therefore, lies about half-way between $\epsilon_{+/0}$ and $\epsilon_{0/-}$ for each structure. The *thermal* excitation energy $\epsilon^{\text{th}}_{+/0}$ is defined to be the total-energy difference between the *relaxed* positive and *relaxed* neutral defect, and similarly for $\epsilon^{\text{th}}_{0/-}$. [$\epsilon^{\text{th}}_{+/0}$ and $\epsilon^{\text{th}}_{0/-}$ are identical to ϵ_1 and ϵ_2 of Eq. (1).] The thermal levels would correspond to ex-

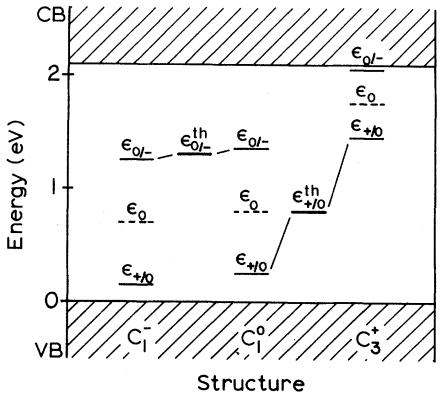

FIG. 7. Possible scenario for location of defect-related energy levels in the gap. C_1^-, C_1^0, and C_3^+ refer to *structures* defined as the relaxed structure for a given charge state. The optical levels $\epsilon_{+/0}$ and $\epsilon_{0/-}$ (light lines) indicate transitions at the given structure, while the thermal levels $\epsilon^{th}_{+/0}$ and $\epsilon^{th}_{0/-}$ (heavy lines) allow structural relaxations. Levels ϵ_0 (dashed lines) represent neutral mean-field eigenvalues. The zero of energy is chosen arbitrarily to lie at the top of the valence band.

perimentally measured activation energies, e.g., for carrier detrapping.

The locations of the various levels in Fig. 7 are based upon the following pieces of evidence. (1) The C_1^0 defect was previously found to have a gap state just below midgap; this determines $\epsilon_0(C_1^0)$. (2) $\epsilon_{0/-}(C_1^0)$ and $\epsilon_{+/0}(C_1^0)$ should lie $\sim U_{el}/2$ above and below $\epsilon_0(C_1^0)$, respectively, where $U_{el}=U_{Coul}+U_{sp}\approx 1.1$ eV (see Fig. 6). (3) The energy levels for C_1^- should lie close to those of C_1^0, because the structures are very similar. They should lie slightly lower because adding an electron to the gap state provides a driving force to lower the gap state. (4) $\epsilon^{th}_{0/-}$ must lie between $\epsilon_{0/-}(C_1^-)$ and $\epsilon_{0/-}(C_1^0)$; in the harmonic approximation, it lies midway between. (5) The total-energy difference between neutral and charged configurations, holding the structure fixed at $C_1^-C_3^+$, is ~ 0.2 eV from Fig. 6. This places $\epsilon_{+/0}(C_3^+)$ 0.2 eV above $\epsilon_{0/-}(C_1^-)$. (6) The C_1^0 defect was previously found[14] to have a defect state below the conduction-band edge. Also, $U_{el}(C_3^+)$ is expected to be smaller than $U_{el}(C_1^-)$, because the defect states are more delocalized.[14] This helps place $\epsilon_0(C_3^+)$ and $\epsilon_{0/-}(C_3^+)$. (That the latter lies in the gap, as shown in Fig. 7, is by no means certain.) (7) Finally, $U_{eff}=\epsilon^{th}_{0/-}-\epsilon^{th}_{+/0}\approx 0.5$ eV determines the location of $\epsilon^{th}_{+/0}$; it is reassuring that the position of this level with respect to $\epsilon_{+/0}(C_3^+)$ and $\epsilon_{+/0}(C_1^0)$ is quite reasonable.

The resulting energy-level diagram is speculative but instructive. In particular, it is quite tempting to associate the thermal levels $\epsilon^{th}_{+/0}$ and $\epsilon^{th}_{0/-}$ with the deep hole and electron trap manifolds found in the xerographic spectroscopy measurements of Abkowitz and Enck (AE).[21] The latter are narrow manifolds, separated by ~ 0.2 eV, centered near midgap, and having an integrated trap density of $\sim 10^{14}$ cm^{-3}. Furthermore, the deep traps of AE appear to be structural in origin; the number of traps (but not their spectral distribution) can be increased by annealing above the glass transition temperature and then quenching to room temperature. Moreover, the excess populations of hole and electron traps subsequently anneal away at the same rate, indicating that the same defect may be reasonable for both traps.

If $C_1^0\rightarrow C_3^+$ and $C_1^0\rightarrow C_1^-$ do in fact correspond to the deep hole and electron trapping processes of AE, this would indicate $U_{eff}\approx +0.2$ eV, although this value is sensitive to the choice of 2.1 eV for the mobility gap.[21] Also, the density of C_1^0 must be $\sim 10^{14}$ cm^{-3}, which is not inconsistent with upper bounds on free spins, as mentioned previously. The density of C_1^0 defects frozen in at the glass transition temperature $T_g=310$ K is expected to be[9]

$$n\approx n_0\exp[-E_{tot}(C_1^0)/kT_g] \tag{12}$$

or $\sim 10^{10}$ cm^{-3} using $E_{tot}(C_1^0)=0.8$ eV from this work. However, an error of a few tenths of an eV in $E_{tot}(C_1^0)$ could shift n by several orders of magnitude because of the exponential in Eq. (12); thus we do not feel that the identification of C_1^0 with the deep traps of AE is ruled out on this basis.

This work does not appear to explain the nature of the more numerous shallow electron and hole traps in Se, which also appear to be of structural origin.[25] We have previously speculated[14] that these transport states might be assigned to intimate valence-alternation pairs.[9]

Finally, we do not think it likely that the C_1^0 center discussed here is related to the photoluminescence[6] (PL) and photoinduced electron-spin resonance[5] (PESR) centers reported in the literature. First, $U_{eff}>0$ implies that the defects initially have a free spin, so that no PESR mechanism is available. Second, the densities of PESR and PL centers have been estimated as $\sim 10^{16}$ cm^{-3} (Ref. 5) and $\gtrsim 10^{15}$ cm^{-3} (Ref. 26), respectively. This appears too large to be consistent with the deep traps of AE, and probably too large for our $E_{tot}(C_1^0)$. Third, the PL efficiency and PESR intensity are both much more sensitive to the presence of impurities in Se than in the compound glasses.[27] Nevertheless, Fig. 7 indicates that the PL process $C_1^0+\gamma\rightarrow C_3^++e^-\rightarrow C_1^0+\gamma$ has an excitation threshold near band gap and a Stokes shift of about half-band gap, which is consistent with PL experiments.[6] (The smaller relaxations for $C_1^0\leftrightarrow C_1^-$ indicate a much smaller

Stokes shift on this side.)

We should like to end this section by emphasizing the need to discriminate carefully between g-Se and the compound chalcogenide glasses. Experimentally, there are numerous striking differences.[28] The photoinduced properties are different in several respects: The PL efficiency and PESR intensity are much lower for Se (Refs. 6, 26, and 27) and show a much stronger sensitivity to impurities (especially O, Ref. 27), the scaling of the PL peak position with band gap evident in the compound chalcogenides breaks down for Se (Ref. 6), and the optically induced below-gap absorption which accompanies the induced ESR in most chalcogenides is either weak or absent in Se.[5] There are also contrasts in the transport properties: Se is unusual in being ambipolar, and its dc electrical conductivity is much more highly impurity dependent (e.g., to O, Cl, and K) than that of the compound glasses.[29] As mentioned above, g-Se has a much lower dielectric constant than the other glasses, and the density of midgap states implied by various experimental measurements is much lower.

Theoretically, we have previously compared g-Se and g-As_2Se_3 and shown that the origin and nature of deep gap states are expected to be quite different for the two cases.[24] For example, the C_1^0 has a deep-gap state because of a unique π interaction between the dangling p orbital and the lone pair on the neighboring atom; this cannot occur for a simple dangling bond in g-As_2Se_3, because the neighboring As atom has no free lone-pair orbitals. Instead, deep states can arise from unique bond orbitals (Se-Se or As-As bonds or As lone pairs) in g-As_2Se_3, where the electronegativity difference between the two constituents plays an important role.

In short, g-Se is anomalous in many respects; in fact, Fritzsche has suggested[30] that the intrinsic defect concentration may be quite low in Se and that most experiments may be governed by impurities. Nonetheless, g-Se is potentially a simpler model system than the compound chalcogenides, because of the much smaller number of possible intrinsic structural defects that must be considered. It appears unlikely that the much more complex compound chalcogenides can be well understood, in terms of specific defects, until further experimental work focused specifically on g-Se provides the answers for this simpler system.

V. SUMMARY

By calculating total energies and Hellman-Feynman forces in the local-density and frozen-core approximations, we have investigated the properties of simple coordination defects in g-Se. Two different model superlattice structures were constructed containing the relevant defects, to ensure that the details of the geometry are not crucial to the results. The method is the same as that of paper II, except that three new corrections are introduced in order to handle charged defects and eliminate interdefect interactions. First, the charge configuration is chosen by using a density-matrix formalism, which also effectively eliminates the interdefect hybridization interactions. Second, interdefect Coulomb interactions are estimated as a Madelung sum and are subtracted out. Third, a spin-polarization correction is introduced to model distant neutral defects.

We verify that the simple bonding defects with charge -1, 0, and $+1$ adopt the structures C_1^-, C_1^0, and C_3^+, respectively, as expected. The structural relaxations between C_1^- and C_1^0 are very small, whereas those for $C_1^0 \leftrightarrow C_3^+$ are much larger, involving formation of an extraordinary bond. Moreover, we find that the structural relaxation at this threefold-coordinated site makes a sizable negative contribution of approximately -0.5 eV to U_{eff}, in agreement with the defect model. However, the repulsive Coulomb interactions give rise to a *larger* positive electronic contribution of approximately $+1.0$ eV, implying an overall positive U_{eff} of approximately $+0.5$ eV.

Because of the low dielectric constant of g-Se and the highly localized nature of the gap state at C_1^-, the present results could still be perfectly consistent with a negative U_{eff} for the compound chalcogenides. In fact, an examination of the experments suggests that the evidence for a negative U is much stronger in the compound glasses. In particular, the density of deep midgap states appears to be low enough in g-Se to fall within the bounds on free spins from ESR measurements. Finally, we obtain a tentative picture of the locations in the gap of various energy levels associated with the structural defects, and compare with the results of xerographic and optical experiments.

ACKNOWLEDGMENTS

This work was supported through the MIT Center for Materials Science and Engineering via National Science Foundation (NSF) Grant No. DMR-76-80895. Additional Berkeley support in the latter stages of the work was provided by NSF Grant No. DMR-78-22465 and by the Director, Office of Energy Research, Office of Basic Energy Sciences, Materials Sciences Division of the U.S. Department of

Energy under Contract No. DE-AC03-76SF00098. The authors (D.V. and J.D.J.) would also like to thank the Miller Institute and the John S. Guggenheim Foundation, respectively, for receipt of fellowships. Finally, it is a pleasure to thank M. Kastner, M. L. Cohen, D. Adler, and M. Abkowitz for many helpful discussions.

[1]N. F. Mott and E. A. Davis, *Electronic Processes in Non-Crystalline Materials* (Clarendon, Oxford, 1971).
[2]H. Fritzsche, in *Amorphous and Liquid Semiconductors,* edited by J. Tauc (Plenum, New York, 1973), p. 221.
[3]J. M. Marshall and E. A. Owen, Philos. Mag. 31, 1341 (1975).
[4]S. C. Agarwal, Phys. Rev. B 7, 685 (1973).
[5]S. G. Bishop, U. Strom, and P. C. Taylor, Phys. Rev. B 15, 2278 (1977); Phys. Rev. Lett. 34, 1346 (1975).
[6]R. A. Street, Adv. Phys. 25, 397 (1976).
[7]P. W. Anderson, Phys. Rev. Lett. 34, 953 (1975).
[8]R. A. Street and N. F. Mott, Phys. Rev. Lett. 35, 1293 (1975); N. F. Mott, E. A. Davis, and R. A. Street, Philos. Mag. 32, 961 (1975).
[9]M. Kastner, D. Adler, and H. Fritzsche, Phys. Rev. Lett. 37, 1504 (1976); M. Kastner and H. Fritzsche, Philos. Mag. B 37, 199 (1978).
[10]P. W. Anderson, J. Phys. (Paris) Colloq. Suppl. No. 10 C4-339 (1976).
[11]D. C. Licciardello, Comm. Solid State Phys. 9, 217 (1980).
[12]D. Emin, J. Non-Cryst. Solids 35-36, 969 (1980), and references therein.
[13]D. Vanderbilt and J. D. Joannopoulos, Solid State Commun. 35, 535 (1980).
[14]D. Vanderbilt and J. D. Joannopoulos, Phys. Rev. B 22, 2927 (1980).
[15](a) D. Vanderbilt and J. D. Joannopoulos, this issue, Phys. Rev. B 27, 6296 (1983); (b) preceding paper, 27, 6302 (1983).
[16]D. Vanderbilt and J. D. Joannopoulos, Phys. Rev. B 26, 5203 (1982).
[17]J. H. Levine and S. G. Louie, Phys. Rev. B 25, 6310 (1982).
[18]L. Hedin and B. I. Lundquist, J. Phys. C 4, 2064 (1971).
[19]H. P. D. Lanyon, Phys. Rev. 130, 134 (1963).
[20]P. Nielsen, Phys. Rev. B 6, 3739 (1972).
[21]M. Abkowitz and R. C. Enck, Phys. Rev. B 25, 2567 (1982).
[22]K. F. Young and H. P. R. Frederikse, J. Phys. Chem. Ref. Data 2, 313 (1973).
[23]B. T. Kolomiets, Phys. Status Solidi 7, 713 (1964).
[24]D. Vanderbilt and J. D. Joannopoulos, Phys. Rev. B 23, 2596 (1981).
[25]M. Abkowitz and R. C. Enck, J. Non-Cryst. Solids 35-36, 831 (1980).
[26]R. A. Street, T. M. Searle, and I. G. Austin, Philos. Mag. 29, 1157 (1974).
[27]S. G. Bishop, U. Strom, E. J. Friebele, and P. C. Taylor, J. Non-Cryst. Solids 32, 359 (1979).
[28]This summary is borrowed in part from S. G. Bishop, U. Strom, and P. C. Taylor, in *The Physics of Selenium and Tellurium,* edited by E. Gerlach and P. Grosse (Springer, New York, 1979), p. 193.
[29]V. A. Twaddle, W. C. LaCourse, and J. D. Mackenzie, J. Non-Cryst. Solids 8-10, 831 (1972).
[30]H. Fritzsche, in *Proceedings of the VIIth International Conference on Amorphous and Liquid Semiconductors,* edited by W. E. Spear (University of Edinburgh, England, 1977), p. 3.